Structure and stability of the (001) alpha-quartz surface

Article (Published Version)

Structure and stability of the (001) α-quartz surface†

T. P. M. Goumans,[a] Adrian Wander,[b] Wendy A. Brown*[a] and
C. Richard A. Catlow[ac]

The structure and surface energies of the cleaved, reconstructed, and fully hydroxylated (001) α-quartz surface of various thicknesses are investigated with periodic density functional theory (DFT). The properties of the cleaved and hydroxylated surface are reproduced with a slab thickness of 18 atomic layers, while a thicker 27-layer slab is necessary for the reconstructed surface. The performance of the hybrid DFT functional B3LYP, using an atomic basis set, is compared with the generalised gradient approximation, PBE, employing plane waves. Both methodologies give similar structures and surface energies for the cleaved and reconstructed surfaces, which validates studying these surfaces with hybrid DFT. However, there is a slight difference between the PBE and B3LYP approach for the geometry of the hydrogen bonded network on the hydroxylated surface. The PBE adsorption energy of CO on a surface silanol site is in good agreement with experimental values, suggesting that this method is more accurate for hydrogen bonded structures than B3LYP. New hybrid functionals, however, yield improved weak interactions. Since these functionals also give superior activation energies, we recommend applying the new functionals to contemporary issues involving the silica surface and adsorbates on this surface.

Introduction

Silica (SiO_2) surfaces are important in a wide range of disciplines.[1] The biotoxicity of silica probably originates from the reactivity of surface sites, specifically silanol groups and undercoordinated silicon and oxygen atoms.[2,3] Furthermore, silica's surface properties are of paramount importance in a variety of technological applications.[1,4] The dissolution and precipitation of the common mineral quartz are major geochemical processes and have therefore been widely investigated.[5] The interaction of molecules with silica(te) surfaces has also been studied because of the catalytic role that dust grains are thought to play in astrochemistry.[6,7]

Despite the importance of silica surfaces in these areas, there is very little detailed experimental structural information. Silica is an insulator, which renders unfeasible several surface techniques routinely applied to conducting surfaces. Nevertheless, it is possible to probe the surface with atomic force microscopy (AFM) and low-energy electron diffraction (LEED). AFM studies have shown that α-quartz has a flat (terraced) surface, but no detailed structural information was determined.[8,9] A LEED study of the α-quartz (001) surface gave a (1 × 1) pattern.[10] However, again no detailed structure was inferred. A complex reconstructed LEED pattern emerges above 873 K, which is attributed to the α → β-quartz phase transition that occurs at 846 K. NMR,[11] ESR,[12] IR,[13] and X-ray photoelectron spectroscopy (XPS)[14] have also been used to identify specific, reactive surface sites such as silanones, silanols and ring structures,[1] but again no detailed structural information has been deduced from these studies.

Due to this lack of detailed experimental data, various computational studies have been performed to investigate the properties of silica surfaces.[15–20] The interactions of amorphous and crystalline silica surfaces with water[21,22] and other interfaces[23] have also been studied computationally. Knowledge of the interactions of the interfaces is of prime importance in understanding silica's toxicology and geochemistry, as well as improving its applications in catalysis and (opto)electronics.

Modelling studies have employed interatomic potential (force field) methods as well as periodic density functional methods. The ionic core-shell model[24] has been particularly successful in describing the structures and relative energies of different silica morphologies[25,26] and surfaces.[20] Interatomic potential methods cannot in general describe bond breaking and formation that takes place in transition states.[22] Electronic structure methods can, however, model chemical reactions and are employed in this study. In particular we use periodic density functional theory (DFT), which has been widely applied in modelling surface structures and reactivities.[21,23,27] All periodic DFT studies of the quartz surface have used either local density (LDA) or generalised gradient approximations (GGA) within a plane wave approach. The CRYSTAL

[a] Chemistry Department, University College London, 20 Gordon Street, London, UK WC1H 0AJ. E-mail: t.goumans@ucl.ac.uk, w.a.brown@ucl.ac.uk; Fax: +44 20 7679 7463; Tel: +44 20 7679 1003
[b] CCLRC Daresbury Laboratory, Keckwick Lane, Warrington, Cheshire, UK WA4 4AD. E-mail: a.wander@dl.ac.uk; Fax: +44 1925 603634; Tel: +44 1925 603652
[c] Davy Faraday Research Laboratory, The Royal Institution of Great Britain, 21 Albemarle Street, London, UK W1X 4BS. E-mail: richard@ri.ac.uk; Fax: +44 20 7670 2920; Tel: +44 (0)20 7670 2901
† Electronic supplementary information (ESI) available: Structures of surfaces and PW91 energies. See DOI: 10.1039/b701176h

programme[28] uses a linear combination of atomic orbitals (LCAO) approach, which facilitates the use of hybrid functionals. Hybrid functionals are popular due to their accurate determination of geometries and energies.[29] Furthermore, new functionals are constantly under development and there are now hybrid functionals that can investigate problems that were notoriously difficult for DFT, such as hydrogen bonds, physisorption[30] and activation barriers.[31] The present work uses the CRYSTAL code,[28] which employs atom-centred basis sets and in which these new functionals will be implemented in the future.[32] In the present study we compare hybrid DFT (B3LYP)[33] employing an atomic basis set with plane wave GGA (PBE)[34] calculations of the structures and energies of silica surfaces.

α-Quartz is the most stable polymorph of silica (SiO_2) at ambient conditions and the (001) surface is the most stable surface as predicted by both interatomic potential[20] and DFT methods.[19] We study the structure and stability of the cleaved, reconstructed and hydroxylated surface of various thicknesses with different density functionals. The convergence of surface structures and energies with slab thicknesses determines the minimum surface depth for future computational studies. The heat of adsorption of CO on the hydroxylated surface is also calculated.

Computational details

The PBE calculations have been performed with CASTEP[35] and the B3LYP calculations with the CRYSTAL03 code.[28] A $4 \times 4 \times 4$ Monkhorst–Pack[36] k-point grid was used for the bulk and a $4 \times 4 \times 1$ grid was used for the surfaces. Adsorption energies were calculated using a 2×2 supercell, sampled with a $2 \times 2 \times 1$ k-point grid.

For the B3LYP calculations two basis sets, 6-31G*[37] and a larger triple zeta basis set,[38] were used. Increased integral accuracies (7 7 7 7 15) and an extra large integration grid were used throughout. Cell and ionic positions were optimised iteratively for the bulk structure of α-quartz. Symmetric adsorption of CO on both sides was used to avoid a spurious dipole moment normal to the surface. Basis set superposition errors were corrected with a counterpoise scheme.[39]

The plane wave calculations were performed with the new ultrasoft pseudopotentials suggested for silicates[40] at a cut-off energy of 700 eV. The absolute energy was well converged (to within a few meV) at this k-point grid and cut-off. For the bulk calculations, both cell parameters and ionic positions were optimised simultaneously, until the forces were less than 0.01 eV per atom. For surface calculations a vacuum gap of about 10 Å was used. Most previous periodic DFT studies

used either LDA or PW91[41] functionals. We employ the PBE functional here, however, because of its good performance for hydrogen bonded systems.[30] PW91 calculations were performed on bulk α-quartz, the 18-layer cleaved and hydroxylated and the 27-layer reconstructed surface to check against our PBE calculations (structures and energies available as supporting information†). The surface structures and energies given by PW91 and PBE calculations are very similar, giving confidence that the results are not specific to our choice of the PBE functional.

For both CASTEP and CRYSTAL, symmetric surfaces with multiple numbers of the bulk unit cell (containing three formula units) were cut, yielding unit cells with 18, 27 and 36 layers of atoms. Initial geometries for the reconstructed surfaces were generated with the GULP code,[42] employing Si and O potentials from Sanders et al.[25] augmented with parameters for the silanol group determined by de Leeuw et al.,[20] while constraining the cell parameters to those of the bulk structure at the respective DFT level.

Results

Bulk structure

α-Quartz is the stable polymorph of SiO_2 at room temperature and low pressure. The silicon atoms are four-coordinated in a network of corner-sharing SiO_4 tetrahedra. The crystal has a hexagonal structure with space group $P3_121$. There are two distinct Si–O bonds with slightly different bond lengths. All Si–O–Si angles are symmetry equivalent, but there are four different O–Si–O angles, which are all very close to the ideal tetrahedral value of 109.45°. All calculated O–Si–O angles are also close to the tetrahedral value and are not reported here. In Table 1 we present the calculated lattice parameters, bond lengths and Si–O–Si bond angles for PBE, PW91 and B3LYP optimised α-quartz. Experimental values are also included in the table for comparison.[43]

The GGA and B3LYP structures are in close agreement with each other. However, both approaches predict approximately 2% larger lattice parameters than are observed experimentally, in agreement with previous calculations.[17,44,45] The B3LYP Si–O–Si angles deviate slightly less from the experimental values than the PBE ones, resulting in slightly less expanded lattices. Usually hybrid DFT calculations predict better geometries[29] and newer functionals may give even better results. Calculations using GGA functionals tend to overestimate bond distances,[29] which accounts for the larger calculated Si–O bond lengths, and resulting expanded lattice

Table 1 Experimental and calculated lattice parameters (a and c), Si–O bond lengths and Si–O–Si angles of α-quartz

Property	PBE	PW91	B3LYP/S[a]	B3LYP/L[b]	Exp.[c]
a/Å	5.052	5.056	5.003	5.010	4.916
c/Å	5.547	5.561	5.504	5.498	5.4054
r(Si–O)/Å	1.630	1.629	1.634	1.632	1.605
	1.633	1.632	1.637	1.635	1.614
$\angle$ (Si–O–Si)/°	147.9	148.6	144.19	144.71	143.73

[a] 6-31G* basis. [b] Large basis (see computational details). [c] Ref. 43.

This journal is © the Owner Societies 2007

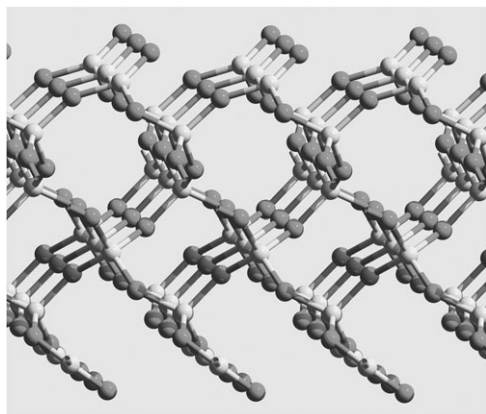*Phys. Chem. Chem. Phys.*, 2007, **9**, 2146–2152 | 2147

Fig. 1 Cleaved α-quartz (001) surface (18 layers), displaying the $Q^2(O)$ sites. Light spheres: Si, dark spheres: O.

parameters, of α-quartz. A similar effect is observed at the B3LYP level, where the Si–O bonds are even longer.

Surfaces

In a recent study of unrelaxed surfaces, relevant to fracturing and therefore to silica's biotoxicity, the (101) surface of α-quartz was found to be the most stable with a surface energy of 2.59 J m^{-2}.[17] When the atoms are relaxed, however, the (001) plane is the most stable surface.[16,19,20] The freshly cleaved (001) surface contains reactive, undercoordinated sites, known as $Q^2(O)$ sites, that consist of a trivalent silicon atom bonded to a protruding singly coordinated oxygen atom (Fig. 1).

Previous molecular dynamics calculations have shown that the cleaved surface undergoes a reconstruction. With DFT (LDA) this transition occurs at 300 K,[19] while with interatomic potential based calculations it occurs above 400 K.[16] In the reconstruction, the surface silicon and oxygen atoms that were undercoordinated in the cleaved surface recover their full coordination, forming six-membered rings (6 Si–O units) parallel to the surface and three-membered rings extending into the bulk (Fig. 2). This reconstruction is commensurate with the α-quartz lattice and therefore the observed (1 × 1) LEED pattern of the α-quartz (001) surface could be due to either the cleaved or the reconstructed surface.[10] Prior to the
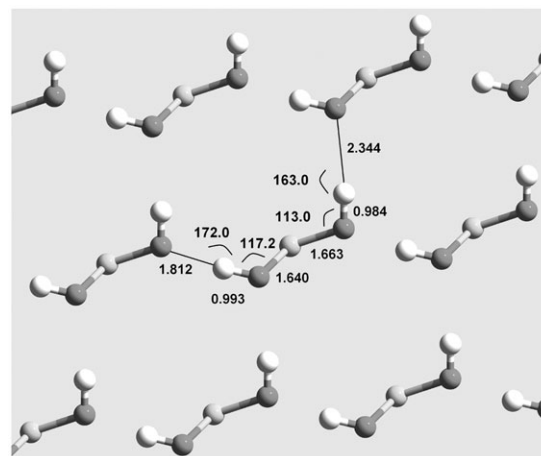

Fig. 3 Hydroxylated α-quartz (001) surface, showing distances and angles of the 18-layered surface at the PBE-level. For clarity, only surface disilanols are shown. Light spheres: Si, dark spheres: O. white spheres: H.

LEED study, the sample was annealed at 773 K, which according to the calculations should be sufficient to produce the reconstructed surface.[16,19] The experimentally observed complex LEED pattern that emerges near 900 K is more probably due to the α → β-quartz phase transition.[10]

Undercoordinated surface sites on silica surfaces are very hydrophilic, reacting quickly with atmospheric water, yielding silanol groups.[46] The surface density of silanol groups on various silica surfaces is 4.5–6.2 per nm^2 under ambient conditions.[46] Previous calculations have shown that the cleaved (001) α-quartz surface reacts exothermically with water molecules until it is fully hydroxylated ($\sim$10 silanol groups per nm^2).[19–21] The fully hydroxylated surface has a zigzag hydrogen bonded network with short and long hydrogen bonds (Fig. 3).

The structure and stability of the cleaved, reconstructed and fully hydroxylated α-quartz (001) surfaces are calculated with GGA and hybrid DFT. Surfaces of 18, 27 and 36 layers of atoms are considered to assess which surface depth is necessary to assure convergence of structure and stability. The computed distances and angles of the surface sites are reported
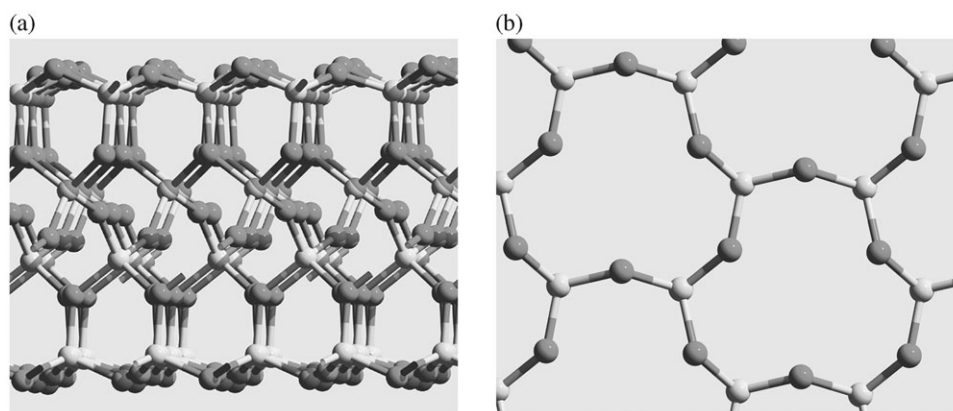

Fig. 2 Reconstructed α-quartz (001) surface, from side (left, 18 layers) and top (right, showing only top Si and O atoms for clarity). Colours as in Fig. 1.

Table 2 Selected bond lengths and angles of α-quartz (001) surface sites on the cleaved, reconstructed and hydroxylated surface consisting of 18, 27 and 36 atomic layers. The coordination of the atoms on the cleaved surface is indicated in the subscript

Bond or angle	PBE	B3LYP/S[a]	B3LYP/L[b]	PBE	B3LYP/S[a]	B3LYP/L[b]	PBE	B3LYP/S[a]	B3LYP/L[b]
	Cleaved, 18 layers			Cleaved, 27 layers			Cleaved, 36 layers		
$r(^3Si-^1O)/Å$	1.530	1.523	1.525	1.530	1.523	1.525	1.530	1.523	1.525
$r(^3Si-^2O)/Å$	1.612	1.614	1.610	1.612	1.614	1.610	1.612	1.614	1.610
	1.640	1.642	1.638	1.641	1.642	1.637	1.640	1.642	1.637
$\angle(^1O-^3Si-^2O)/°$	125.9	126.5	125.8	125.9	126.4	125.8	126.2	126.5	126.0
	126.9	127.2	127.2	127.0	127.2	127.2	126.9	127.2	127.3
	Reconstructed, 18 layers			Reconstructed, 27 layers			Reconstructed, 36 layers		
$r(Si-O)^c/Å$	1.621	1.623	1.620	1.622	1.622	1.618	1.621	1.622	1.618
	1.628	1.628	1.625	1.628	1.630	1.626	1.629	1.630	1.627
	1.634	1.633	1.630	1.632	1.633	1.630	1.633	1.633	1.630
$\angle(Si-O-Si)/°(6MR)^d$	122.0	121.0	121.4	121.9	120.8	121.2	121.9	120.8	121.2
	130.2	127.2	128.1	127.1	124.8	125.3	127.3	125.0	125.7
	130.3	127.3	128.2	133.7	130.1	131.5	133.5	129.9	131.8
$\angle(Si-O-Si)/°(3MR)^e$	129.1	130.1	130.6	128.5	127.8	128.5	128.2	128.0	128.6
	130.1	130.8	130.7	132.2	131.9	132.6	131.8	131.7	132.5
	Hydroxylated, 18 layers			Hydroxylated, 27 layers			Hydroxylated, 36 layers		
$r(O-H)/Å$	0.984	0.982	0.983	0.982	0.982	0.983	0.984	0.982	0.983
	0.993	0.986	0.988	0.992	0.986	0.988	0.994	0.986	0.988
$r(H\cdots O)/Å$	1.812	1.855	1.846	1.797	1.850	1.835	1.802	1.849	1.836
	2.344	2.177	2.256	2.380	2.186	2.275	2.359	2.187	2.273
$r(Si-O)/Å$	1.640	1.646	1.641	1.639	1.645	1.640	1.639	1.645	1.640
	1.663	1.661	1.658	1.664	1.662	1.658	1.664	1.662	1.658
$\angle(O-H\cdots O)/°$	163.8	168.9	165.8	163.1	168.8	165.6	163.2	168.6	165.7
	172.0	169.2	169.0	172.3	169.1	168.9	172.3	169.1	168.9
$\angle(Si-O-H)/°$	113.0	112.5	113.4	113.1	112.5	113.4	113.0	112.5	113.3
	117.3	115.3	116.1	117.5	115.4	116.3	117.4	115.4	116.2

[a] 6-31G* basis. [b] Large basis (see computational details). [c] Averaged over two distances. [d] In three-membered ring. [e] In six-membered ring.

in Table 2 and full structures are available as ESI.† The surface energies of all of the surfaces considered are presented in Table 3.

Cleaved surface

The geometry of the reactive $Q^2(O)$ site on the cleaved surface hardly changes with either increasing surface depth or DFT method. All calculated distances and angles are the same within 0.5% (Table 2). Together with the constant surface energy (Table 3), this indicates that the cleaved surface can be accurately modelled with a relatively thin, symmetric 18-layer Si_6O_{12} slab.

The cleaved surface has a high surface energy (2.2–2.4 J m^{-2}), rendering this surface very reactive. Therefore, a freshly cut α-quartz (001) surface will quickly reconstruct or react with gas phase or solvent molecules. As noted, the high reactivity of cleaved silica surfaces may underlie its biotoxicity. Hybrid DFT calculations could provide insight into the detailed workings of silica's biotoxicity by assessing the interactions between biomolecules and the cleaved surfaces.

Reconstructed surface

The structure of the reconstructed surface has been calculated previously by Rigagnese *et al.* with LDA.[19] At that level, the Si–O bond distances in the six-membered ring are all very similar (1.58–1.60 Å), but with PBE and B3LYP three different groups of distances are calculated, as seen in Table 2. The LDA distances are smaller than those calculated here because of the overbinding that occurs with LDA.[29] However, the Si–O bond distances are in very good agreement with each other for the PBE and B3LYP calculations, as was also observed for the cleaved surface. Apparently, the

Table 3 Surface energies of cleaved, reconstructed and hydroxylated α-quartz (001) surfaces of various thicknesses

Surface	Depth	PBE/J m^{-2}	B3LYP/S[a]/J m^{-2}	B3LYP/L[b]/J m^{-2}
Cleaved	18 layers	2.21	2.37	2.30
	27 layers	2.22	2.37	2.30
	36 layers	2.22	2.37	2.31
Reconstructed	18 layers	0.31	0.46	0.43
	27 layers	0.36	0.53	0.49
	36 layers	0.36	0.52	0.49
Hydroxylated[c]	18 layers	−0.19	−0.34	−0.15
	27 layers	−0.19	−0.34	−0.14
	36 layers	−0.19	−0.34	−0.14

[a] 6-31G* basis. [b] Large basis (see computational details). [c] Surface stability with respect to bulk + H_2O (g). For H_2O (l) add 0.34 J m^{-2}.

This journal is © the Owner Societies 2007

Phys. Chem. Chem. Phys., 2007, **9**, 2146–2152 | 2149

characteristics of the Si–O bond are very similar within the PBE and B3LYP approaches, although, as noted, the calculated Si–O bonds in the bulk structure are slightly enlarged with respect to the experimental values (Table 1).

The Si–O–Si angles in the strained six-membered and three-membered rings are smaller than the bulk values, while the O–Si–O angles remain close to the ideal tetrahedral value, reflecting the softer bending mode of Si–O–Si. There is a small difference between the calculated Si–O–Si angles at the PBE and B3LYP level, with B3LYP predicting smaller values, closer to the experimental values, at least for the bulk structure (Table 1).

The reconstruction distorts at least the top six layers of atoms and, consequently, the calculated surface energies depend on the depth of the reconstructed surface. Both sides of the 18-layer slab are in close proximity, leading to a slight shortening of the central Si–O bonds (see structures provided in the ESI†). This shortening artificially stabilises the thinnest surface slab with respect to the others (Table 3). Since spiro compounds, where two rings are joined at a common atom, are stabilised by heavy (P, Si) atoms,[47] the overstabilisation in the thin layer may be due to the (too) close proximity of the protruding three-membered rings. There are also small differences between the surface Si–O–Si angles for the thinnest slab and the thicker ones.

The reconstructed surface satisfies all oxygen and silicon valencies, which stabilises it significantly, by about 1.9 J m^{-2}, with respect to the cleaved surface. GGA predicts a slightly higher stability than B3LYP (surface energies 0.36 vs. 0.5 J m^{-2}). However, because there are no experimental surface energies for α-quartz with which to compare our calculations, it is impossible to decide which functional performs better, although hybrid functionals tend to predict more accurate energies than GGA functionals.[29] Because the 27- and 36-layer surfaces have very similar geometries and energies, it is suggested that 27-layer slabs are used for studying processes on the reconstructed (001) α-quartz surface.

Hydroxylated surface

Previous calculations on the fully hydroxylated α-quartz surface revealed its herringbone structure (Fig. 3).[19–21] Although the Si–O distances are again very consistent between GGA and hybrid DFT, there are significant differences in the geometries of the silanol hydrogen bonded network (Table 2). The H···O hydrogen bonds have the greatest variations amongst the methods and surface depths, which is a consequence of the soft vibrational modes in hydrogen bonded networks,[48] and illustrates the fact that various density functionals perform differently for hydrogen bonds.[30]

The hydroxylated surface has one long and one short hydrogen bond, in agreement with which PBE predicts one hydrogen bond to be about 1.80 Å and the other about 2.35 Å. At the B3LYP level the short hydrogen bond is slightly longer (∼ 1.85 Å), and the long hydrogen bond is slightly shorter, but that distance also depends significantly on the choice of basis set (Table 2). The O–H distances differ much less than the hydrogen bond lengths, with PBE distances being about 0.984 and 0.993 Å and B3LYP distances being slightly shorter (0.982 and 0.987 Å). The calculated PW91 structure and stability of the 18-layer surface is very similar to the PBE one (see full structures provided in the ESI†).

The hydroxylated α-quartz (001) surface is much more stable than the dry surfaces, confirming the known strong hydrophilicity of quartz surfaces. The surface energy is independent of surface depth, although the different functionals predict different values for the surface energies, as seen in Table 3. Weak interactions, such as hydrogen bonds, are notoriously difficult for density functional methods to calculate. The accuracy of a given functional also depends on the choice of basis set. Zhao and Truhlar recently compiled a benchmarking database of weakly interacting systems for testing functionals.[30] From their study, it transpired that PBE with a large basis set is a good method for describing hydrogen bonded systems,[30] while B3LYP is much less accurate. Therefore, we suggest that adsorption studies on the hydroxylated surface should employ PBE with an 18-layer surface slab. The best overall hybrid functional for hydrogen bonded systems is B3P86,[30] although mPWB1K[49] and B97-1[50] perform similarly well. The latter two functionals provide more accurate activation energies[30,31] and their future implementation in CRYSTAL would provide an accurate method for describing reactions on the hydroxylated surface of quartz.

CO adsorption

The adsorption of CO on the 18-layer hydroxylated α-quartz (001) surface has been calculated with PBE and with B3LYP using a large basis. Carbon monoxide adsorbs preferentially with the C-end hydrogen bonded to a surface silanol that previously was involved in a long hydrogen bond. The adsorption energies are 13.4 and 8.6 kJ mol^{-1} at the PBE and B3LYP/Large levels, respectively. The calculated PBE value is in good agreement with the experimental adsorption enthalpy of CO on silica (11 kJ mol^{-1})[51] and on ground comet material rich in silicates (13.5 kJ mol^{-1}).[6] PBE energies of hydrogen bonded systems are more accurate than B3LYP energies, as previously observed by Zhao and Truhlar.[30] This supports our earlier suggestion that PBE is the method of choice for calculations on hydrogen bonded systems while awaiting the availability of new functionals such as B97-1 and mPWB1K that can adequately deal with hydrogen bonds as well as transition states.

Conclusions

The geometry and stability of cleaved, reconstructed and fully hydroxylated α-quartz (001) surfaces of 18, 27 and 36 layers of atoms are studied using PBE with a plane wave basis and B3LYP with two atomic basis sets. The PBE results are consistent with PW91 calculations for selected surfaces. The properties of the cleaved and reconstructed surfaces are very similar with either method. The two approaches differ, however, in their prediction of the hydrogen bond distances on the hydroxylated surface. The surface structure and energy of the cleaved and hydroxylated surfaces are independent of slab thickness, suggesting that 18-layer slabs are sufficient to encompass the full properties of these surfaces. However, for

2150 | *Phys. Chem. Chem. Phys.*, 2007, **9**, 2146–2152

This journal is © the Owner Societies 2007

the reconstructed surface the properties are only converged at a thickness of 27 layers.

The cleaved surface has a large surface energy (2.2–2.4 J m^{-2}), rendering it very reactive. The reactive site, $Q^2(O)$, consists of a tricoordinated silicon atom and a monocoordinated oxygen atom, which readily reacts with an adjacent $Q^2(O)$ site or with water to yield the reconstructed or the fully hydroxylated surface, respectively. Reconstruction leads to the formation of six-membered rings parallel and on top of the surface, along with protruding three-membered rings, which leads to significant differences in both geometry and energy between the 18-layer slab and the thicker slabs. The 27- and 36-layer slabs have very similar geometries and surface energies, hence the surface properties are converged at a thickness of 27 layers. The reconstructed surface is stabilised by $\sim$1.9 J m^{-2} with respect to the pristine cleaved surface. The fully hydroxylated surface has a hydrogen bonded network with one short and one long hydrogen bond. The PBE and B3LYP approaches have different hydrogen bond lengths, with the PBE predicting the short hydrogen bond to be shorter and the longer to be longer than B3LYP. The hydroxylated surface is very stable, confirming the extreme hydrophilicity of pristine silica surfaces. The adsorption energy of CO on the hydroxylated surface is calculated to be 13.4 kJ mol^{-1} with PBE, in accord with experiments. The B3LYP/Large adsorption energy is slightly lower, at 8.6 kJ mol^{-1}.

Based on our findings we advocate using 18-layer surface slabs for calculations of adsorption on, or reactions with, the cleaved and fully hydroxylated α-quartz surfaces. The reconstructed surface, however, should be at least 27 layers thick to avoid unwanted effects on the surface properties. The PBE functional is the method of choice for adsorption on the hydroxylated surface until new functionals are implemented in CRYSTAL. Otherwise, we recommend using hybrid functionals when studying processes on the α-quartz surface, especially with new and future functionals that can adequately deal with activation barriers and weak interactions.

Acknowledgements

References

1 *The Surface Properties of Silica*, ed. A. P. Legrand, John Wiley, New York, 1998.
2 T. Nash, A. C. Alison and J. S. Harington, *Nature*, 1966, **211**, 259.
3 V. V. Murashov, M. Harper and E. Demchuk, *J. Occup. Environ. Hyg.*, 2006, **3**, 718.
4 (*a*) *The Physics and Chemistry of SiO₂ and the Si–SiO₂ Interface*, ed. C. R. Helms and B. E. Deal, Plenum Press, New York, 1988; (*b*) *The Physics and Chemistry of SiO₂ and the Si–SiO₂ Interface 2*, ed. C. R. Helms and B. E. Deal, Plenum Press, New York, 1993.
5 (*a*) J. D. Rimstidt and H. L. Barnes, *Geochim. Cosmochim. Acta*, 1980, **44**, 1683; (*b*) K. A. Pisciotto, *Sedimentology*, 1980, **28**, 547; (*c*) W. A. House and D. R. Orr, *J. Chem. Soc., Faraday Trans.*, 1992, **88**, 233; (*d*) F. Jedoubi, A. Mgaidi and M. El Maaoui, *Can. J. Chem. Eng.*, 1998, **76**, 233; (*e*) P. M. Dove, *Geochim. Cosmochim. Acta*, 1999, **63**, 3715; (*f*) V. A. Alekseyev, L. S. Medvedeva and Y.

G. Tatsii, *Geochem. Int*, 2003, **41**, 459; (*g*) W. L. Huang, *Eur. J. Mineral.*, 2003, **15**, 843; (*h*) J. E. Greenwood, V. W. Truesdale and A. R. Rendell, *Aquat. Geochem.*, 2005, **11**, 1; (*i*) S. Y. Yanina, K. M. Rosso and P. Meakin, *Geochim. Cosmochim. Acta*, 2006, **70**, 1113.
6 M. N. Mautner, V. Abdelsayed, M. S. El-Shall, J. D. Thrower, S. D. Green, M. P. Collings and M. R. S. McCoustra, *Faraday Discuss.*, 2006, **133**, 103.
7 H. J. Fraser, S. E. Bisschop, K. M. Pontoppidan, A. G. G. M. Tielens and E. F. van Dishoeck, *Mon. Not. R. Astron. Soc.*, 2005, **356**, 1283.
8 S. Noge, A. Nobushige, K. Komine, H. Suzuki, H. Shiraishi and K. Hohkawa, *Jpn. J. Appl. Phys.*, 1997, **36**, 3081.
9 M. L. Schlegel, K. L. Nagy, P. Fenter and N. C. Sturchio, *Geochim. Cosmochim. Acta*, 2002, **66**, 3037.
10 F. Bart and M. Gautier, *Surf. Sci.*, 1994, **311**, L671.
11 A. S. Zyubin, A. M. Mebel, S. H. Lin and Y. D. Glinka, *J. Chem. Phys.*, 2002, **116**, 9889.
12 G. Hochstrasser and J. F. Antonini, *Surf. Sci.*, 1972, **32**, 644.
13 V. A. Radtsig, I. V. Berestetskaya and S. N. Kostritsa, *Kinet. Katal.*, 1998, **6**, 863.
14 Y. Duval, J. A. Mielczarski, O. S. Pokrovsky, E. Mielczarski and J. J. Erhardt, *J. Phys. Chem. B*, 2002, **106**, 2937.
15 D. A. Litton and S. H. Garofalini, *J. Non-Cryst. Solids*, 1997, **217**, 250.
16 M. V. Koudriachova, J. V. L. Beckers and S. W. de Leeuw, *Comput. Mater. Sci.*, 2001, **20**, 381.
17 (*a*) V. V. Murashov and E. Demchuk, *J. Phys. Chem. B*, 2005, **109**, 10835; (*b*) V. V. Murashov, *J. Phys. Chem. B*, 2005, **109**, 4144.
18 E. Chagarov, A. A. Demkov and J. B. Adams, *Phys. Rev. B*, 2005, **71**, 075417.
19 (*a*) G.-M. Rigagnese, A. De Vita, J.-C. Charlier, X. Gonze and R. Car, *Phys. Rev. B*, 2000, **61**, 13250; (*b*) G.-M. Rigagnese, PhD Thesis, Université Catholique de Louvain, 1998.
20 N. H. de Leeuw, F. M. Higgins and S. C. Parker, *J. Phys. Chem. B*, 1999, **103**, 1270.
21 (*a*) T. R. Walsh, M. Wilson and A. P. Sutton, *J. Chem. Phys.*, 2000, **113**, 9191; (*b*) G.-M. Rigagnese, J.-C. Charlier and X. Gonze, *Phys. Chem. Chem. Phys.*, 2004, **6**, 1920; (*c*) M.-H. Du, A. Kolchin and H.-P. Cheng, *J. Chem. Phys.*, 2004, **120**, 1044; (*d*) E. A. Leed, J. O. Sofo and C. G. Pantano, *Phys. Rev. B*, 2005, **72**, 155427; (*e*) C. Mischler, J. Horbach, W. Kob and K. Binder, *J. Phys.: Condens. Matter*, 2005, **17**, 4005; (*f*) J. Yang, S. Meng, L. Xu and E. G. Wang, *Phys. Rev. B*, 2005, **71**, 035413; (*g*) J. Yang and E. G. Wang, *Phys. Rev. B*, 2006, **72**, 035406.
22 Z. Du and N. H. de Leeuw, *Dalton Trans.*, 2006, 2623.
23 (*a*) L. Giordano, D. Ricci, G. Pacchioni and P. Ugliengo, *Surf. Sci.*, 2005, **584**, 225; (*b*) J. Weissenrieder, S. Kaya, J.-L. Lu, H.-J. Gao, S. Shaikhutdinov, H.-J. Freund, M. Sierka, T. K. Todorova and J. Sauer, *Phys. Rev. Lett.*, 2005, **95**, 076103; (*c*) K. D. Kwon, V. Vadillo-Rodriguez, B. E. Logan and J. D. Kubicki, *Geochim. Cosmochim. Acta*, 2006, **70**, 3803; (*d*) X. Solans-Monfort, J. S. Filhol, C. Coperet and O. Eisenstein, *New J. Chem.*, 2006, **30**, 842.
24 B. G. Dick, Jr and A. W. Overhauser, *Phys. Rev.*, 1958, **112**, 90.
25 M. G. Sanders, M. Leslie and C. R. A. Catlow, *J. Chem. Soc., Chem. Commun.*, 1984, 1271.
26 P. Tangney and S. Scandolo, *J. Chem. Phys.*, 2002, **117**, 8898.
27 (*a*) M. Neurock, in *Dynamics Of Surfaces And Reaction Kinetics In Heterogeneous Catalysis*, ed. G. F. Froment and K. C. Waugh, Elsevier, Amsterdam, 1997; (*b*) V. Milman, B. Winkler, J. A. White, C. J. Pickard, M. C. Payne, E. V. Akhmatskaya and R. H. Nobes, *Int. J. Quantum Chem.*, 2000, **77**, 895; (*c*) A. Mingani and F. Illas, *J. Phys. Chem. B*, 2006, **110**, 11894.
28 V. R. Saunders, R. Dovesi, C. Roetti, R. Orlando, C. M. Zicovich-Wilson, N. M. Harrison, K. Doll, B. Civalleri, I. J. Bush, Ph. D'Arco and M. Llunell, CRYSTAL03.
29 *A Chemist's Guide to Density Functional Theory*, ed. W. Koch and M. C. Holthausen, Wiley-VCH, Weinheim, 2000.
30 (*a*) Y. Zhao and D. G. Truhlar, *J. Chem. Theory Comput.*, 2005, **1**, 415; (*b*) Y. Zhao and D. G. Truhlar, *J. Phys. Chem. A*, 2005, **109**, 5656.
31 S. Andersson and M. Grüning, *J. Phys. Chem. A*, 2004, **108**, 7621.
32 N. M. Harrison, private communication.

33 (*a*) A. D. Becke, *J. Chem. Phys.*, 1993, **98**, 5648; (*b*) C. Lee, W. Yang and R. G. Parr, *Phys. Rev. B*, 1988, **37**, 785.

34 J. P. Perdew, K. Burke and M. Ernzerhof, *Phys. Rev. Lett.*, 1996, **77**, 3865.

35 M. D. Segall, P. J. D. Lindan, M. J. Probert, C. J. Pickard, P. J. Hasnip, S. J. Clark and M. C. Payne, CASTEP 4.0, *J. Phys.: Condens. Matter*, 2002, **14**, 2717.

36 H. J. Monkhorst and J. D. Pack, *Phys. Rev. B*, 1976, **13**, 5188.

37 (*a*) P. C. Hariharan and J. A. Pople, *Theor. Chim. Acta*, 1972, **28**, 213; (*b*) M. M. Francl, W. J. Pietro, W. J. Hehre, J. S. Binkley, M. S. Gordon, D. J. DeFrees and J. A. Pople, *J. Chem. Phys.*, 1982, **77**, 3654.

38 http://www.tcm.phy.cam.ac.uk/~mdt26/crystal.html, 'large basis' for Si, '88-411G(*)' for O and third contraction (~8-21G**) for H.

39 S. F. Boys and F. Bernardi, *Mol. Phys.*, 1970, **19**, 553.

40 B. Civalleri and N. M. Harrison, *Mol. Simul.*, 2002, **28**, 213.

41 Y. Wang and J. P. Perdew, *Phys. Rev. B*, 1991, **44**, 13298.

42 J. D. Gale, *J. Chem. Soc., Faraday Trans.*, 1997, **93**, 629.

43 L. Levien, C. T. Prewitt and D. J. Weidner, *Am. Mineral.*, 1980, **65**, 920.

44 C. M. Zicoivch-Wilson, F. Pascale, C. Roetti, V. R. Saunders, R. Orlando and R. Dovesi, *J. Comput. Chem.*, 2004, **25**, 1873.

45 Th. Demuth, Y. Jeanvoine, J. Hafner and J. G. Ángyán, *J. Phys.: Condens. Matter*, 1999, **11**, 3833.

46 *The Chemistry of Silica*, ed. R. K. Iler, John Wiley, New York, 1979.

47 (*a*) T. Iwamoto, M. Tamura, C. Kabuto and M. Kira, *Science*, 2000, **290**, 504; (*b*) M. J. M. Vlaar, M. H. Lor, A. W. Ehlers, M. Schakel, M. Lutz, A. L Spek and K. Lammertsma, *J. Org. Chem.*, 2002, **67**, 2485.

48 C. Lee, D. Vanderbilt, R. Car and M. Parrinello, *Phys. Rev. B*, 1993, **47**, 4863.

49 Y. Zhao and D. G. Truhlar, *J. Phys. Chem. A*, 2004, **108**, 6908.

50 F. A. Hamprecht, A. J. Cohen, D. J. Tozer and N. C. Handy, *J. Chem. Phys.*, 1998, **109**, 6264.

51 T. P. Beebe and J. T. Yates, *Surf. Sci.*, 1983, **159**, 369.